

---

# Learn from Global Correlations: Enhancing Evolutionary Algorithm via Spectral GNN

---

**Kaichen Ouyang**

University of Science and Technology of China  
Hefei, China  
oykc@mail.ustc.edu.cn

**Shengwei Fu**

Guizhou University  
Guizhou, China  
gs.swfu22@gzu.edu.cn

**Zong Ke**

National University of Singapore  
Singapore  
a0129009@u.nus.edu

**Renxiang Guan**

National University of Defense Technology  
Hunan, China  
lhpang.xidian@gmail.com

**Ke Liang**

National University of Defense Technology  
Hunan, China  
liangke200694@126.com

**Dayu Hu\***

National University of Defense Technology  
Hunan, China  
hudayu@nudt.edu.cn

## Abstract

Evolutionary algorithms (EAs) are optimization algorithms that simulate natural selection and genetic mechanisms. Despite advancements, existing EAs have two main issues: (1) they rarely update next-generation individuals based on global correlations, thus limiting comprehensive learning; (2) it is challenging to balance exploration and exploitation, excessive exploitation leads to premature convergence to local optima, while excessive exploration results in an excessively slow search. Existing EAs heavily rely on manual parameter settings, inappropriate parameters might disrupt the exploration-exploitation balance, further impairing model performance. To address these challenges, we propose a novel evolutionary algorithm framework called Graph Neural Evolution (GNE). Unlike traditional EAs, GNE represents the population as a graph, where nodes correspond to individuals, and edges capture their relationships, thus effectively leveraging global information. Meanwhile, GNE utilizes spectral graph neural networks (GNNs) to decompose evolutionary signals into their frequency components and designs a filtering function to fuse these components. High-frequency components capture diverse global information, while low-frequency components capture more consistent information. This explicit frequency filtering strategy directly controls global-scale features through frequency components, overcoming the limitations of manual parameter settings and making the exploration-exploitation control more interpretable and effective. Extensive evaluations on nine benchmark functions (e.g., Sphere, Rastrigin, and Rosenbrock) demonstrate that GNE consistently outperforms both classical algorithms (GA, DE, CMA-ES) and advanced algorithms (SDAES, RL-SHADE) under various conditions, including original, noise-corrupted, and optimal solution deviation scenarios. GNE achieves solution quality several orders of magnitude better than other algorithms (e.g.,  $3.07e-20$  mean on Sphere vs.  $1.51e-07$ ).

---

\*Corresponding author

# 1 Introduction

Graph Neural Networks (GNNs) have been widely applied in fields such as social network analysis, recommendation systems, and protein structure prediction because of their capacity to effectively model complex relational structures using graph representations[1–5]. In GNNs, dependencies between nodes are captured by propagating and aggregating information across the network, thereby enabling adaptive learning and optimization based on node interactions. Similarly, biological evolution involves genetic interactions characterized by variation, recombination, and natural selection, which are processes that collectively facilitate the evolutionary optimization of genotypes toward greater fitness[6–8]. Given these parallels, we propose that GNNs can be understood through an evolutionary perspective, where the propagation of information among nodes mirrors the diversity-exploring mechanisms of crossover and mutation, as well as the adaptive optimization mechanism of directional selection in evolution.

Evolutionary adaptation thrives on two complementary strategies: exploration through genetic diversity (e.g., avian wing polymorphism spanning short, medium, and long morphotypes) and exploitation via trait optimization[9–11]. Consider three avian archetypes: short-winged penguins excel in aquatic foraging, medium-winged gulls balance aerial maneuverability with diving efficiency, and long-winged albatrosses dominate transoceanic flight—each adaptation emerging from mutation-driven exploration and sustained through environmental selection. Similarly, giraffes’ neck elongation, refined iteratively over generations, exemplifies exploitation’s role in amplifying fitness-critical traits. Evolutionary algorithms (EAs) formalize this duality: crossover/mutation operators probe global solution spaces (exploration), while selection pressures refine local optima (exploitation)[12–14].

Conventional EAs fail to fully exploit the global relationships among individuals in a population, relying on limited information from a few individuals for updating a single solution[15, 10, 16], thus hindering comprehensive learning. Additionally, existing EAs optimize functions in a black-box manner, with parameter selection relying on extensive experimental results. Inappropriate parameter choices can easily disrupt the balance between exploration and exploitation, potentially leading to suboptimal results [17–19]. To address these limitations, we reinterpret evolutionary algorithms through a GNN lens, proposing Graph Neural Evolution (GNE). In GNE, each candidate solution in population is represented as a node in a graph, with the corresponding value in the adjacency matrix between two nodes reflecting the similarity of them. This approach fully leverages global correlations among individuals within the population, overcoming the constraints of local updates. These global correlations resemble biological reproductive isolation, where genetically similar individuals preferentially exchange traits[20]. Moreover, we compute the normalized Laplacian matrix from the population’s adjacency matrix and decompose it into frequency components through its eigenvalues and eigenvectors in the spectral domain. Similar to spectral GNNs, GNE balances high-frequency exploration (diverse traits) and low-frequency exploitation (consistent traits) via filter functions. Notably, this explicit spectral aggregation strategy can control global-scale features through frequency components, making the exploration–exploitation control both interpretable and effective.

This spectral perspective provides a unified mathematical framework: the balance between exploration and exploitation in evolutionary algorithms is equivalent to designing an appropriate filter that assigns suitable weights to the different frequency components of the population, where strengthening the high-frequency components corresponds to reinforcing exploration behavior, and strengthening the low-frequency components corresponds to reinforcing exploitation behavior. By formalizing this duality, GNE provides interpretable control over the exploration-exploitation balance while benefiting from global correlations. Through rigorous evaluations on nine benchmark functions (e.g., Sphere, Rastrigin, and Rosenbrock), GNE consistently outperforms classical algorithms, including Genetic Algorithm (GA) [12], Differential Evolution (DE) [14], Covariance Matrix Adaptation Evolution Strategy (CMA-ES) [21], and advanced algorithms such as Evolution Strategy Based on Search Direction Adaptation (SDAES) [22] and Learning Adaptive Differential Evolution by Natural Evolution Strategies (RL-SHADE) [23] across scenarios with original, noise-corrupted, and deviated-optimum conditions. GNE leads other algorithms by multiple orders of magnitude in solution quality (e.g.,  $3.07e-20$  vs.  $1.51e-07$  mean on Sphere). This framework is broadly applicable to complex optimization problems in the real world, such as engineering design, and optimization of parameters and architecture of neural networks[24–26]. To summarize, our contributions are threefold:

**Problem.** We discuss the intrinsic duality between Spectral GNNs and EAs. To the best of our knowledge, this is the first comprehensive study focusing on graph neural evolution.

**Algorithm.** Different from existing EAs, we construct an adjacency matrix to capture global correlations within the population. The global evolutionary signals are decomposed into their frequency components in the spectral domain and then fused via bespoke filter functions. This explicit spectral aggregation strategy can control global features through frequency components, making the exploration-exploitation control both interpretable and effective.

**Evaluation.** Extensive empirical studies have been conducted on nine representative benchmark functions to evaluate the performance of GNE. The experimental results demonstrate that it can effectively learn from global correlations and balance exploration and exploitation, thereby significantly outperforming existing EAs in terms of accuracy, convergence, stability, and robustness.

## 2 Related Works

The proposed GNE framework integrates EAs with the GNNs by modeling population dynamics as spectral graph operations. We first review related works on EAs and GNNs, identifying gaps that motivate GNE.

**Evolutionary Algorithms.** EAs are a family of metaheuristic optimization techniques inspired by natural evolutionary processes, incorporating operators such as natural selection and mutation. GA is one of the earliest and most representative EAs, and is particularly effective in solving discrete and multimodal optimization problems[12]. In recent years, DE[14, 16, 27] and Evolution Strategy (ES)[28–30] have emerged as prominent research domains. DE generates candidate solutions through differential mutation and selects the fittest among them. Numerous variants have been developed, including Adaptive Differential Evolution with Optional External Archive (JADE) [31], which incorporates external archives and adaptive parameter updates; Success-History Based Parameter Adaptation for Differential Evolution (SHADE) [32], which utilizes historically successful parameter settings to refine control parameters; and RL-SHADE [23], which further enhances DE performance by integrating natural evolution strategies for more effective parameter optimization. Among ES methods, Covariance Matrix Adaptation Evolution Strategy (CMA-ES) is one of the most widely recognized algorithms [21], adjusting the covariance matrix to effectively explore the solution space. Several variants have been developed, including OpenES for large-scale parallel computation [33]; Parameter-Exploring Policy Gradients (PEPG) for estimating gradients in the parameter space [34]; Mixture Model based Evolution Strategy (MMES) [35], which accelerates CMA-ES in large-scale optimization tasks; and SDAES [22], which reduces both time and space complexity in high-dimensional settings. From GA to DE, ES, and their variants, the design of evolutionary algorithms has consistently centered on balancing exploration and exploitation. Exploration introduces diversity to expand the search space and prevent premature convergence to local optima, while exploitation refines promising solutions to gradually approach the global optimum[9].

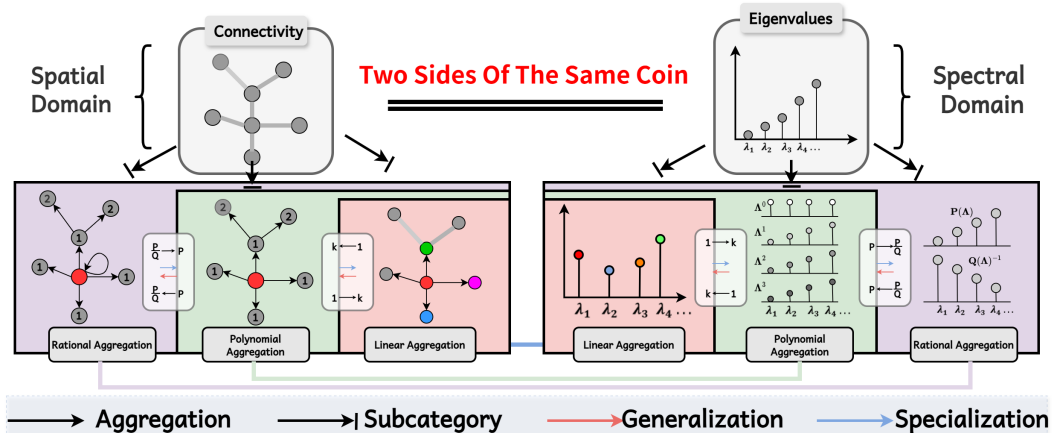


Figure 1: The relationship between spatial and spectral domain graph neural networks.

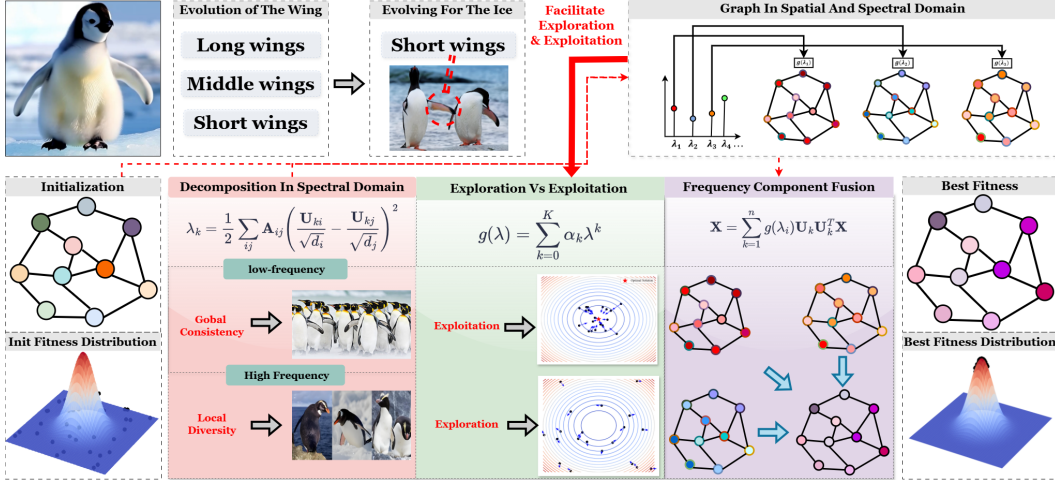


Figure 2: The framework of the proposed GNE method. It begins by constructing the population’s adjacency matrix to capture global relationships, which is computed using cosine similarities between individual nodes. The obtained adjacency matrix is further transformed into the graph Laplacian. Through this process, GNE extracts frequency components that characterize population diversity (high-frequency) and consistency (low-frequency). Furthermore, exploration–exploitation balance is achieved by modulating the weights of these frequency components with a polynomial filter, while a sampling function resamples the population in feature space to optimize overall fitness.

**Graph Neural Networks.** GNNs process graph-structured data from two principal perspectives: spatial and spectral[36–38]. Spatial GNNs are more widely known, with the Graph Convolutional Network (GCN) [1] being a representative example, which aggregates information from neighboring nodes to learn local structures. The Graph Attention Network (GAT) [2] further enhances GCNs by incorporating self-attention mechanisms, while GraphSAGE generates node embeddings by sampling and aggregating features from local neighborhoods, thereby enabling generalization to previously unseen nodes [5]. In contrast, spectral GNNs rely on the graph Laplacian and Fourier transform for convolution operations, thus learning from global structural patterns. Here we review representative spectral methods. ChebyNet introduces Chebyshev polynomials to construct efficient spectral filters, thereby improving scalability [39]. BernNet learns spectral filters through Bernstein polynomial approximations, which provide flexibility in filter design and help overcome the limitations of predefined or unconstrained filters [40]. JacobiConv increases expressive power by employing an orthogonal Jacobi basis, yielding superior performance over other spectral GNNs across both synthetic and real-world datasets [38]. In brief, spectral GNNs derive filtering expressions that modulate both the low-frequency and high-frequency components of the original graph signals. This process aligns with evolutionary dynamics: low-frequency components represent the stable core of the graph signal, while high-frequency components capture variations among nodes, thereby capturing finer details.

**Bridging the Gap.** Prior efforts rarely unify EAs and GNNs. Conventional EAs are black-box methods and ignore graph-structured interactions, while GNNs focus on representation learning rather than evolutionary optimization. Our work addresses this gap by reinterpreting EA dynamics as spectral graph filtering, enabling explicit control over exploration–exploitation through frequency modulation using filter functions.

### 3 Evolution via Spectral Graph Representations

#### 3.1 Preliminary

**Notations.** Given a set of nodes  $\mathcal{V} = \{v_1, \dots, v_N\}$ , an undirected graph can be represented in matrix form as  $\mathcal{G} = (\mathbf{X}, \mathbf{A})$ , where the adjacency matrix  $\mathbf{A} \in \mathbb{R}^{N \times N}$  encodes the pairwise interactions between nodes. The degree matrix  $\mathbf{D} \in \mathbb{R}^{N \times N}$  is defined as  $\mathbf{D}_{ii} = \sum_j \mathbf{A}_{ij}$ , and the normalized Laplacian matrix is presented as  $\hat{\mathbf{L}} = \mathbf{I} - \mathbf{D}^{-\frac{1}{2}} \mathbf{A} \mathbf{D}^{-\frac{1}{2}}$ . This matrix can also be expanded in the spectral form as  $\hat{\mathbf{L}} = \mathbf{U} \mathbf{\Lambda} \mathbf{U}^\top$ , where  $\mathbf{U}$  contains orthonormal eigenvectors and  $\mathbf{\Lambda} = \text{diag}(\lambda_1, \dots, \lambda_N)$  is a diagonal matrix of the corresponding eigenvalues, which satisfy  $\lambda_k \in [0, 2]$ . The graph Fourier transform is defined as  $\tilde{\mathbf{X}} = \mathbf{U}^\top \mathbf{X}$ , with inverse transform  $\mathbf{X} =$

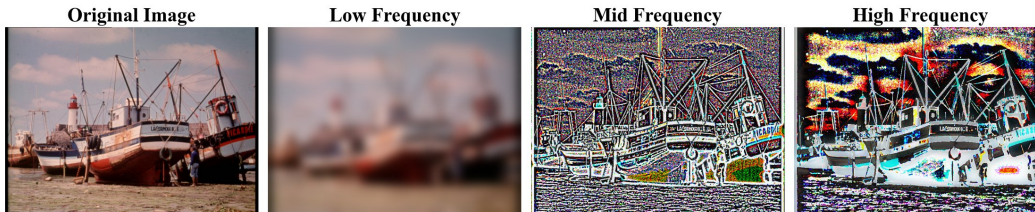


Figure 3: Visualizing the relationship between consistent traits (low-frequency) and diverse traits (high-frequency) in the Boat.

$\mathbf{U}\tilde{\mathbf{X}}$ . The component at frequency  $\lambda_k$  is given by  $\tilde{\mathbf{X}}_{\lambda_k} = \mathbf{U}_k \mathbf{U}_k^\top \mathbf{X}$ , where  $\mathbf{U}_k$  is the eigenvector corresponding to  $\lambda_k$ . The spectral filter is defined as  $g(\mathbf{\Lambda}) = \text{diag}(g(\lambda_1), \dots, g(\lambda_N))$  and is generally parameterized by a  $k$ th-order polynomial,  $g(\lambda) = \sum_{k=0}^K \alpha_k \lambda^k$ , which lifts to the vertex domain through  $g(\hat{\mathbf{L}}) = \mathbf{U}g(\mathbf{\Lambda})\mathbf{U}^\top$ .

**Problem formulation.** In the proposed GNE framework, the evolution of the population can be regarded as a frequency filtering process. By controlling the frequency components, the balance between exploration and exploitation is achieved. Specifically, the GNE population-update procedure is based on a polynomial filter and can be defined as follows:

$$g(\hat{\mathbf{L}}) \mathbf{X} = \mathbf{U} g(\mathbf{\Lambda}) \mathbf{U}^\top \mathbf{X} = \sum_{k=1}^n g(\lambda_k) \mathbf{U}_k \mathbf{U}_k^\top \mathbf{X} = \sum_{k=1}^n g(\lambda_k) \tilde{\mathbf{X}}_{\lambda_k}, \quad (1)$$

Here,  $\mathbf{X}$  is integrated with the filtering function  $g(\cdot)$  to produce the next generation of the population. This carefully designed population-update method introduces frequency regulation into the evolutionary framework, thereby rendering the entire update process both interpretable and effective.

### 3.2 The proposed GNE model

Existing representative evolutionary algorithms, such as DE[14], typically operate via three key steps: mutation, crossover, and selection. During the mutation step, a mutant vector  $\mathbf{v}_i$  is generated for each individual  $\mathbf{x}_i$  in the population:

$$\mathbf{v}_i = \mathbf{x}_{r1} + \alpha_s \cdot (\mathbf{x}_{r2} - \mathbf{x}_{r3}), \quad (2)$$

where  $\mathbf{x}_{r1}$ ,  $\mathbf{x}_{r2}$ , and  $\mathbf{x}_{r3}$  denote distinct individuals randomly selected, and  $\alpha_s$  serves as the scaling factor that controls the magnitude of exploration. Then the crossover step generates a trial vector  $\mathbf{u}_i$  by merging components from both the mutant vector  $\mathbf{v}_i$  and the target vector  $\mathbf{x}_i$ :

$$\mathbf{u}_{i,j} = \begin{cases} \mathbf{v}_{i,j} & \text{if } \text{rand}(0, 1) \leq p_{cr} \text{ or } j = j_r \\ \mathbf{x}_{i,j} & \text{otherwise,} \end{cases} \quad (3)$$

where  $p_{cr}$  is the crossover rate determining the probability of inheriting components from the mutant vector, and  $j_r$  ensures that at least one component is inherited from  $\mathbf{v}_i$ . Besides,  $\mathbf{u}_{i,j}$ ,  $\mathbf{v}_{i,j}$  and  $\mathbf{x}_{i,j}$  denote the  $j$ -th components of the trial vector  $\mathbf{u}_i$ , mutant vector  $\mathbf{v}_i$  and target vector  $\mathbf{x}_i$ , respectively. The selection step retains the superior individual between the trial vector  $\mathbf{u}_i$  and the target vector  $\mathbf{x}_i$ :

$$\mathbf{x}'_i = \begin{cases} \mathbf{u}_i & \text{if } f(\mathbf{u}_i) \leq f(\mathbf{x}_i) \\ \mathbf{x}_i & \text{otherwise,} \end{cases} \quad (4)$$

where  $\mathbf{x}'_i$  represents the updated individual for the next generation, and  $f(\cdot)$  denotes the fitness function. Higher values of  $\alpha_s$  and  $p_{cr}$  promote exploration, whereas lower values favor exploitation. However, these operations occur at the individual level, and for specific problem types, the algorithm's performance is sensitive to the choice of  $\alpha_s$  and  $p_{cr}$ . While traditional EAs, such as DE, perform well on many problems, they lack modeling of the global correlations of the population, providing limited direct control and interpretability over the exploration-exploitation trade-off. These limitations may result in instability across different problem types.

To address these limitations, we propose the GNE, which reformulates the EAs within a graph-based framework to capture global correlations (Figure 2). In GNE, individuals are represented as nodes, and their interactions are modeled using an adjacency matrix. The adjacency matrix  $\mathbf{A}$  captures

---

**Algorithm 1** Iterative Algorithm of GNE

- 1: **Input:** Population size  $N$ , maximum number of iterations  $T$ , sampling functions  $\varphi(\cdot)$  and  $\phi(\cdot)$ , spectral filter  $g(\cdot)$ , objective function  $f(\cdot)$ .
  - 2: **Output:** Optimal solution  $\mathbf{x}_{\text{best}}$  and objective value  $f_{\text{best}}$ .
  - 3: Initialize population  $\mathbf{X} = \{\mathbf{x}_1, \dots, \mathbf{x}_N\}$  with random solutions.
  - 4: Evaluate  $f(\mathbf{x}_i)$  for each  $\mathbf{x}_i \in \mathbf{X}$ .
  - 5:  $\mathbf{x}_{\text{best}} \leftarrow \arg \min_{\mathbf{x}_i \in \mathbf{X}} f(\mathbf{x}_i)$ .
  - 6:  $f_{\text{best}} \leftarrow f(\mathbf{x}_{\text{best}})$ .
  - 7: **for**  $t = 1$  **to**  $T$  **do**
  - 8: Encode population with  $\varphi$ :  $\mathbf{X} \leftarrow \varphi(\mathbf{X})$ .
  - 9: Compute similarity matrix  $\mathbf{A}$  from  $\mathbf{X}$ .
  - 10: Compute degree matrix  $\mathbf{D}$  of  $\mathbf{A}$ .
  - 11: Compute normalized Laplacian  $\hat{\mathbf{L}} \leftarrow \mathbf{I} - \mathbf{D}^{-1/2} \mathbf{A} \mathbf{D}^{-1/2}$ .
  - 12: Compute eigen-decomposition  $\hat{\mathbf{L}} = \mathbf{U} \mathbf{\Lambda} \mathbf{U}^\top$ .
  - 13: Update population using spectral filter:  $\hat{\mathbf{X}} \leftarrow \mathbf{U} g(\mathbf{\Lambda}) \mathbf{U}^\top \mathbf{X}$ .
  - 14: Apply encoder  $\phi$  to  $\hat{\mathbf{X}}$ :  $\mathbf{X} \leftarrow \phi(\hat{\mathbf{X}})$ .
  - 15: Evaluate  $f(\mathbf{x}_i)$  for each  $\mathbf{x}_i \in \mathbf{X}$ .
  - 16: Set  $\mathbf{x}' \leftarrow \arg \min_{\mathbf{x}_i \in \mathbf{X}} f(\mathbf{x}_i)$ .
  - 17: **if**  $f(\mathbf{x}') < f_{\text{best}}$  **then**
  - 18:  $\mathbf{x}_{\text{best}} \leftarrow \mathbf{x}'$ .
  - 19:  $f_{\text{best}} \leftarrow f(\mathbf{x}_{\text{best}})$ .
  - 20: **end if**
  - 21: **end for**
  - 22: **Return:**  $\mathbf{x}_{\text{best}}, f_{\text{best}}$ .
- 

the strength of node interactions, prioritizing exchanges among similar individuals, analogous to reproductive isolation mechanisms in biology. This matrix is computed using the cosine similarity between individuals  $i$  and  $j$ , based on their difference vectors  $\mathbf{z}_i = \mathbf{x}_i - \mathbf{x}_0$ , where  $\mathbf{x}_0$  denotes the population centroid. The element  $\mathbf{A}_{ij}$  represents the  $i$ -th row and  $j$ -th column of the adjacency matrix:

$$\mathbf{A}_{ij} = \frac{\mathbf{z}_i \cdot \mathbf{z}_j^\top}{\|\mathbf{z}_i\| \|\mathbf{z}_j\|}. \quad (5)$$

Based on the obtained adjacency matrix, we further compute the normalized graph Laplacian matrix  $\hat{\mathbf{L}} = \mathbf{I} - \mathbf{D}^{-\frac{1}{2}} \mathbf{A} \mathbf{D}^{-\frac{1}{2}}$ , which undergoes spectral decomposition  $\hat{\mathbf{L}} = \mathbf{U} \mathbf{\Lambda} \mathbf{U}^\top$  to generate eigenvalues  $\lambda_k$ , which are given by:

$$\lambda_k = \frac{1}{2} \sum_{ij} \mathbf{A}_{ij} \left( \frac{\mathbf{U}_{ki}}{\sqrt{d_i}} - \frac{\mathbf{U}_{kj}}{\sqrt{d_j}} \right)^2, \quad (6)$$

where  $\mathbf{U}_{ki}$  and  $\mathbf{U}_{kj}$  denote the components of individuals  $i$  and  $j$  in the eigenvector  $\mathbf{U}_k$ , and  $d_i$  and  $d_j$  represent their degrees. The eigenvalues  $\lambda_k$  have a physical meaning as frequencies and quantify the variability along  $\mathbf{U}_k$ . Higher values of  $\lambda_k$  indicate greater variability, with transitions from high to low frequencies reflecting a shift from diverse traits to consistent traits, which aligns with maintaining population diversity in EAs to fully explore the solution space while preserving consistency for fine exploration around the optimal solution. Figure 3 provides a vivid example visualizing this relationship.

By leveraging global correlations encoded in the eigenvalues  $\lambda_k$ , GNE directly regulates the exploration–exploitation trade-off within the population through the polynomial filter function  $g(\lambda) = \sum_{k=0}^K \alpha_k \lambda^k$ , as expressed by the following equation:

$$\hat{\mathbf{X}} = \mathbf{U} g(\mathbf{\Lambda}) \mathbf{U}^\top \mathbf{X} = \sum_{k=1}^n g(\lambda_k) \mathbf{U}_k \mathbf{U}_k^\top \mathbf{X} = \sum_{k=1}^n g(\lambda_k) \tilde{\mathbf{X}}_{\lambda_k}. \quad (7)$$

where the term  $\tilde{\mathbf{X}}_{\lambda_k}$  represents the population's component corresponding to  $\lambda_k$ , while  $g(\lambda_k)$  is the weight applied to this component. Increasing the weight of high-frequency components boosts

Table 1: Performance Comparison of GNE with Other Evolutionary Algorithms on Benchmark Functions

Noise	Function	Non-Graph EAs					Graph EAs
		GA	DE	CMA-ES	SDAES	RL-SHADE	GNE
Without Noise	Sphere	2.31E+04 $\pm$ 7.10E+03	4.53E-04 $\pm$ 1.75E-04	1.22E-05 $\pm$ 9.27E-06	9.22E-18 $\pm$ 1.43E-17	1.51E-07 $\pm$ 2.17E-07	<b>3.07E-20</b> $\pm$ 5.26E-21
	Schwefel	5.60E+01 $\pm$ 8.58E+00	2.31E-03 $\pm$ 5.83E-04	5.28E-03 $\pm$ 1.46E-03	1.54E-06 $\pm$ 5.94E-06	4.14E-04 $\pm$ 4.99E-04	<b>7.65E-10</b> $\pm$ 4.08E-11
	Schwefel 2.22	5.42E+04 $\pm$ 1.38E+04	3.24E+04 $\pm$ 5.31E+03	4.28E-01 $\pm$ 2.33E-01	1.35E-01 $\pm$ 9.86E-02	1.85E+01 $\pm$ 1.51E+01	<b>6.40E-20</b> $\pm$ 1.33E-20
	Schwefel 2.26	7.22E+01 $\pm$ 7.57E+00	1.25E+01 $\pm$ 1.56E+00	2.35E-02 $\pm$ 6.63E-03	2.67E-03 $\pm$ 8.72E-03	5.03E+00 $\pm$ 2.29E+00	<b>6.86E-11</b> $\pm$ 6.04E-12
	Rosenbrock	2.53E+07 $\pm$ 1.57E+07	1.51E+02 $\pm$ 5.00E+01	1.73E+02 $\pm$ 4.19E+02	4.90E+01 $\pm$ 5.87E+01	4.60E+01 $\pm$ 4.01E+01	<b>2.85E+01</b> $\pm$ 4.19E-02
	Quartic	1.16E+01 $\pm$ 7.72E+00	5.84E-02 $\pm$ 1.35E-02	2.64E-02 $\pm$ 5.59E-03	1.31E-01 $\pm$ 5.25E-02	3.74E-02 $\pm$ 1.92E-02	<b>7.24E-05</b> $\pm$ 5.65E-05
	Rastrigin	1.97E+01 $\pm$ 4.50E+01	5.69E-03 $\pm$ 7.74E+00	1.09E-03 $\pm$ 7.24E+01	5.85E+00 $\pm$ 3.22E+01	2.28E+00 $\pm$ 3.99E+00	<b>1.28E-10</b> $\pm$ 0.00E+00
	Ackley	2.06E+02 $\pm$ 5.55E-01	7.85E-03 $\pm$ 1.17E-03	1.72E-04 $\pm$ 2.51E-04	1.07E-03 $\pm$ 9.09E+00	1.00E-02 $\pm$ 6.03E-01	<b>0.00E+00</b> $\pm$ 1.01E-11
	Levy	1.78E+07 $\pm$ 6.49E+01	5.83E-05 $\pm$ 1.08E-02	1.29E-06 $\pm$ 7.96E-05	3.11E-02 $\pm$ 3.40E-03	2.97E-01 $\pm$ 1.03E-02	<b>2.23E-03</b> $\pm$ 0.00E+00
With Noise	Sphere	2.31E+04 $\pm$ 7.44E+03	2.87E-01 $\pm$ 4.21E-02	1.12E-01 $\pm$ 2.67E-02	3.64E-01 $\pm$ 9.54E-02	2.13E-01 $\pm$ 7.92E-02	<b>1.11E-04</b> $\pm$ 8.19E-05
	Schwefel	5.49E+01 $\pm$ 8.94E+00	6.43E-01 $\pm$ 7.48E-02	3.78E-01 $\pm$ 4.18E-02	2.51E+00 $\pm$ 2.29E+00	6.04E-01 $\pm$ 2.95E-01	<b>1.96E-04</b> $\pm$ 1.84E-04
	Schwefel 2.22	5.52E+04 $\pm$ 1.66E+04	3.35E+04 $\pm$ 5.03E+03	6.30E-01 $\pm$ 2.22E-01	8.72E+00 $\pm$ 3.38E+00	1.76E+01 $\pm$ 1.16E+01	<b>9.12E-05</b> $\pm$ 7.37E-05
	Schwefel 2.26	7.27E+01 $\pm$ 9.53E+00	1.58E+01 $\pm$ 2.94E+00	4.10E-01 $\pm$ 2.56E-02	4.54E+00 $\pm$ 2.39E+00	1.04E+01 $\pm$ 3.62E+00	<b>1.56E-04</b> $\pm$ 1.15E-04
	Rosenbrock	2.59E+07 $\pm$ 1.45E+07	1.37E+02 $\pm$ 6.25E+01	4.91E+01 $\pm$ 4.61E+01	9.24E+01 $\pm$ 1.25E+02	5.19E+01 $\pm$ 4.05E+01	<b>2.89E+01</b> $\pm$ 3.56E-02
	Quartic	1.30E+01 $\pm$ 1.11E+01	6.08E-02 $\pm$ 1.58E-02	2.62E-02 $\pm$ 5.59E-03	1.36E-01 $\pm$ 4.78E-02	4.02E-02 $\pm$ 1.79E-02	<b>5.21E-05</b> $\pm$ 4.97E-05
	Rastrigin	2.63E+02 $\pm$ 4.27E+01	8.77E+01 $\pm$ 7.24E+00	1.23E+02 $\pm$ 7.54E+01	1.13E+02 $\pm$ 3.74E+01	1.29E+01 $\pm$ 3.73E+00	<b>1.01E-04</b> $\pm$ 8.86E-05
	Ackley	1.99E+01 $\pm$ 5.99E-01	2.81E+00 $\pm$ 3.51E-01	7.20E+00 $\pm$ 1.00E+01	1.79E+01 $\pm$ 6.89E+00	2.69E+00 $\pm$ 6.96E-01	<b>1.22E-04</b> $\pm$ 9.02E-05
	Levy	1.91E+02 $\pm$ 6.33E+01	1.21E+00 $\pm$ 2.24E-02	1.10E+00 $\pm$ 2.02E-02	1.35E+00 $\pm$ 1.05E-01	1.18E+00 $\pm$ 7.41E-02	<b>8.36E-05</b> $\pm$ 8.64E-05

exploration, while increasing the weight of low-frequency components strengthens exploitation. The updated population  $\hat{\mathbf{X}}$  is obtained by integrating different frequency components.

GNNs typically employ multilayer perceptron (MLP) encoders  $\psi(\cdot)$  and  $\phi(\cdot)$  to transform and map features both before and after filtering, thereby further optimizing node representations. Similarly, GNE treats  $\psi(\cdot)$  and  $\phi(\cdot)$  as sampling functions that guide the population to generate new individuals toward optimizing overall population fitness, this point will be further discussed in Appendix B. To summarize, the overall update formula for GNE can be expressed as follows:

$$\mathbf{X} \leftarrow \phi(\mathbf{U}g(\boldsymbol{\Lambda})\mathbf{U}^\top\psi(\mathbf{X})) \quad (8)$$

To provide an intuitive overview of GNE’s update procedure, Algorithm 1 illustrates the iterative update process.

## 4 Experiments

In this section, we evaluate the performance of GNE, where the filter function is represented using Chebyshev polynomials, against five well-established and widely recognized evolutionary algorithms: GA[12], DE[14], CMA-ES[21], SDAES[22], and RL-SHADE[23]. The comparison is conducted on nine classical benchmark functions to evaluate the convergence and robustness of GNE. Detailed descriptions of these benchmark functions, including their mathematical expressions, bounds, dimensions, and characteristics, are provided in Appendix C.1.

Additionally, we examine GNE’s performance under challenging scenarios, such as when noise is added to the function or when the optimal solution is shifted, to verify its robustness and adaptability in diverse optimization settings. The experiment was conducted using an Intel Core i5-12400 CPU (2.50 GHz), 16 GB of RAM, and the MATLAB 2023a platform for analysis. As an extension, we also analyze the impact of different polynomial bases on GNE’s performance, with the formulations and analysis results of these polynomials presented in Appendix C.2.

### 4.1 Comparison of GNE and Other Evolutionary Algorithms

To validate the effectiveness of GNE, we compare it against classical and advanced evolutionary algorithms (GA, DE, CMA-ES, SDAES, RL-SHADE) on nine benchmark functions: Sphere, Schwefel, Schwefel 2.22, Schwefel 2.26, Rosenbrock, Quartic, Rastrigin, Ackley, and Levy. For each algorithm, the population size  $N$  is set to 30, and the maximum number of iterations  $T$  is set to 500. Each algorithm is independently executed 30 times, and we calculate the mean and standard deviation of the results. Table 1 presents the performance comparison of GNE with other evolutionary algorithms (GA, DE, CMA-ES, SDAES, and RL-SHADE) on various benchmark functions. Across all tested functions, GNE consistently achieves the best results in terms of both mean and standard deviation, highlighting its precision, stability, and robustness. For example, in Sphere, Schwefel, and Schwefel 2.22, GNE significantly outperforms other algorithms, achieving near-zero average values with the smallest standard deviation, demonstrating its ability to converge accurately and stability to the global

optimum. In multi-modal functions such as Rastrigin and Ackley, where the landscape is highly complex with numerous local optima, GNE excels in maintaining a balance between exploration and exploitation, delivering superior accuracy compared to other methods. On Rosenbrock and Levy, GNE outperforms all other algorithms with its ability to adapt to complex optimization spaces, achieving the lowest error and exhibiting exceptional stability. In contrast, other algorithms show varying levels of performance. While DE and CMA-ES generally perform better than GA on most functions, they often struggle to match GNE’s precision and stability. RL-SHADE and SDAES exhibit competitive performance on certain functions, such as Rosenbrock and Ackley, but their results still lack the consistency observed with GNE, particularly in terms of standard deviation, which is crucial for robustness. GA, being the simplest method, demonstrates the weakest performance overall, with higher mean and larger standard deviations across all functions, indicating its limited capacity for handling complex or multi-modal optimization problems.

## 4.2 Robustness of GNE in Noisy Function Environments

In real-world scenarios, function evaluations are often affected by measurement errors and uncertainties [41, 42]. In this section, we introduce random noise uniformly distributed in the range [0, 1] to the nine benchmark functions to evaluate the performance of GNE under noisy function conditions. This setup tests the algorithm’s robustness when noise is present in the computation of function values.

Table 1 highlights the performance of GNE and other evolutionary algorithms (GA, DE, CMA-ES, SDAES, and RL-SHADE) under noisy benchmark functions, showcasing their robustness in handling noisy environments. Compared to the noise-free scenarios in Table 1, the introduction of random noise significantly impacts the performance of most algorithms. GA and SDAES experience severe performance degradation, with large mean and high standard deviations across almost all functions, indicating their inability to effectively handle noise. DE and CMA-ES also show reduced performance, particularly in complex multi-modal functions like Rastrigin-Noise and Ackley-Noise, where noise amplifies the difficulty of optimization. RL-SHADE performs relatively better than most algorithms, but its increased variability under noisy conditions makes its results less reliable. In stark contrast, GNE consistently achieves the smallest averages and standard deviations across all noisy benchmark functions, maintaining its superior performance even in the presence of noise. For example, in functions such as Sphere-Noise, Schwefel-Noise, and Quartic-Noise, GNE significantly outperforms other algorithms, demonstrating its robustness and ability to effectively mitigate the influence of noise. Even in challenging scenarios like Rastrigin-Noise and Ackley-Noise, where noise typically causes significant performance degradation, GNE remains highly accurate and stable. This exceptional robustness can be attributed to GNE’s capture of global correlations within the population, controlling global-scale features through frequency components. It avoids algorithm failure caused by excessive fitness evaluation noise of a few individuals or improper parameter selection, thereby enhancing the algorithm’s adaptability to external environmental uncertainties.

To demonstrate the balance between overall performance and computational time in GNE, Figure 4 presents the Friedman ranking [43] and average running times of different algorithms on benchmark functions under both noise-free and noisy conditions. GA and DE, two classic and simple algorithms, exhibit the shortest running times in both conditions but achieve the lowest rankings. CMA-ES and RL-SHADE rank in the middle under both conditions but require the longest and second-longest running times, respectively. SDAES achieves the shortest running time in the noise-free condition and ranks second, slightly behind GNE. However, in the presence of noise, its optimization efficiency significantly deteriorates, dropping to the second-to-last position, even performing worse than the simple algorithm DE. In contrast, GNE achieves the highest ranking under both noise-free and noisy conditions while using a moderate amount of computational time. Additionally, GNE demonstrates strong adaptability to the optimization of functions with added noise, maintaining robust performance across varying conditions.

## 4.3 Robustness of GNE for Optimal Solution Deviation

A critical problem in benchmarking and analysis of evolutionary computation methods is that many benchmark functions have optima located at the center of the feasible set, which can create biases in the evaluation of evolutionary algorithms [44]. The center-bias in some methods allows them to easily find optima, rendering comparisons with other algorithms that lack such biases ineffective. To address this issue, we study whether the proposed GNE algorithm exhibits overfitting to the optimal solution by testing its performance under varying deviations. The optimal solution is intentionally shifted

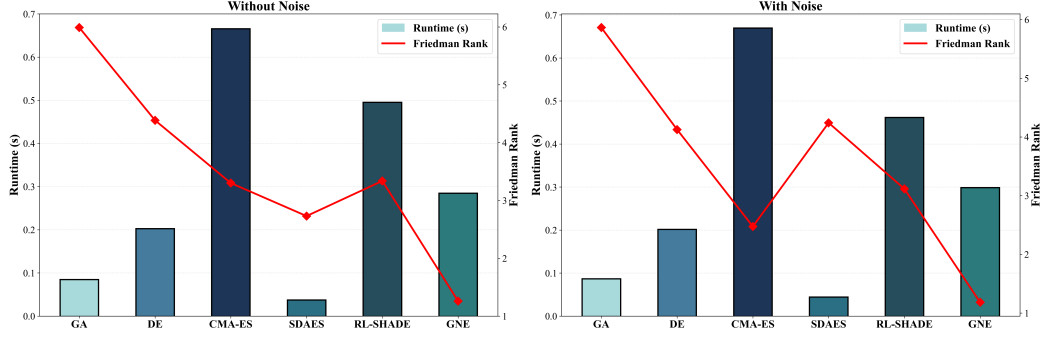


Figure 4: Comparison of the runtime and Friedman ranking of different algorithms on the benchmark function

Table 2: Performance Comparison of GNE with Other Evolutionary Algorithms on Optimal Solution Deviation Experiment

Deviation	Non-Graph EAs					Graph EAs
	GA	DE	CMA-ES	SDAES	RL-SHADE	GNE
-10	2.60E+04 ± 7.94E+03	3.94E-04 ± 1.63E-04	1.20E-05 ± 5.67E-06	7.77E-18 ± 9.82E-18	2.17E-07 ± 5.60E-07	<b>4.22E-19 ± 1.33E-19</b>
-30	3.51E+04 ± 1.12E+04	5.49E-04 ± 2.49E-04	1.21E-05 ± 5.81E-06	9.00E-18 ± 1.37E-17	5.84E-08 ± 6.79E-08	<b>4.12E-19 ± 1.12E-19</b>
-50	5.47E+04 ± 1.19E+04	4.01E-04 ± 1.53E-04	1.41E-05 ± 8.43E-06	5.05E-18 ± 6.04E-18	4.55E-07 ± 1.79E-06	<b>3.86E-19 ± 1.17E-19</b>
-70	1.04E+05 ± 2.16E+04	3.49E-04 ± 1.49E-04	1.63E-05 ± 8.97E-06	3.79E-17 ± 9.31E-17	2.03E-07 ± 3.91E-07	<b>4.39E-19 ± 1.26E-19</b>
-90	1.71E+05 ± 2.51E+04	1.31E-04 ± 7.58E-05	1.92E-05 ± 8.10E-06	5.65E-17 ± 1.38E-16	1.15E-07 ± 2.22E-07	<b>4.06E-19 ± 1.00E-19</b>
+10	2.22E+04 ± 8.65E+03	3.97E-04 ± 2.13E-04	1.31E-05 ± 6.11E-06	9.38E-18 ± 1.45E-17	2.16E-07 ± 5.23E-07	<b>4.09E-19 ± 1.01E-19</b>
+30	2.10E+04 ± 8.80E+03	4.88E-04 ± 1.60E-04	1.13E-05 ± 4.82E-06	9.81E-18 ± 1.94E-17	2.71E-07 ± 4.49E-07	<b>4.30E-19 ± 9.91E-20</b>
+50	2.60E+04 ± 1.22E+04	4.60E-04 ± 1.49E-04	1.59E-05 ± 6.11E-06	7.66E-18 ± 9.10E-18	6.21E-07 ± 2.51E-06	<b>4.20E-19 ± 1.20E-19</b>
+70	4.76E+04 ± 1.60E+04	3.36E-04 ± 1.26E-04	1.60E-05 ± 7.53E-06	1.42E-17 ± 2.63E-17	1.09E-07 ± 1.19E-07	<b>3.79E-19 ± 6.79E-20</b>
+90	1.10E+05 ± 2.67E+04	1.42E-04 ± 5.28E-05	1.99E-05 ± 7.86E-06	3.19E-17 ± 7.22E-17	8.24E-08 ± 2.55E-07	<b>3.79E-19 ± 1.55E-19</b>

by deviations of -10, -30, -50, -70, -90, +10, +30, +50, +70, and +90. This setup is designed to test GNE’s robustness when the optimal solution deviates from its original position. Table 2 presents the performance comparison of GNE with other evolutionary algorithms (GA, DE, CMA-ES, SDAES, and RL-SHADE) under different optimal solution deviations in the Sphere function. This highlights the robustness and adaptability of GNE in handling dynamic changes in the solution landscape, thanks to the translation invariance property of its adjacency matrix, which captures global correlations by modeling relative relationships within the population without relying on the boundaries of the solution space, as discussed in Appendix D. Furthermore, GNE guides population updates using global-scale information, mitigating the risk of overfitting caused by the influence of a few individuals on population update.

## 5 Discussion

Here, we provide a summary statement to underscore the paper’s central focus:

(1) The principal contribution of this paper is not only the introduction of a graph-evolution framework but also an explicit-modeling approach that aims to revolutionize existing EAs. Moreover, the study delineates clear directions for future EA research in terms of interpretability, effectiveness, and stability.

(2) Compared with existing EAs, Evolution via Spectral Graph Representations benefits from modeling global correlations. The constructed graph is then decomposed to generate spectral components, which are optimized through a frequency-based filter. This control facilitates an automatic exploration–exploitation balance, in which high-frequency modes encode population diversity, whereas low-frequency modes encode population consistency.

(3) We propose a novel paradigm that bridges two fields and unveils the inherent connection between EAs and spectral GNNs, thereby fostering mutual advancement. For EAs, spectral tools provide richer population modeling and a principled basis for operator design. For GNNs, evolutionary operators inspire adaptive, exploration-aware spectral filters, which in turn suggest new network architectures.

## 6 Conclusion

In this study, we present the GNE framework, which models pairwise relationships within the population by means of an adjacency matrix and captures global correlations via spectral decomposition. Evolutionary signals are encoded into frequency components whose global-scale influence is modulated by a polynomial filter function, thereby rendering the exploration–exploitation balance both interpretable and effective. We demonstrate GNE’s performance on nine benchmark functions (e.g., Sphere, Rastrigin, and Rosenbrock), where it consistently outperforms classical algorithms (GA, DE, CMA-ES) and advanced algorithms (SDAES, RL-SHADE) under various conditions, including noise corruption and deviations from the optimal solution. By synthesizing the experimental results, we demonstrate the effectiveness of GNE within existing evolutionary methods and argue that evolution via spectral graph representations enables explicit modeling of evolutionary processes. Future work will focus on testing GNE’s performance on larger-scale optimization problems, exploring ways to reduce the complexity of spectral decomposition (e.g., adaptive population size reduction), and applying GNE to more real-world optimization problems, such as complex engineering problems and optimization of neural network parameters and structures.

## References

- [1] T. N. Kipf and M. Welling, “Semi-supervised classification with graph convolutional networks,” *arXiv preprint arXiv:1609.02907*, 2016.
- [2] P. Veličković, G. Cucurull, A. Casanova, A. Romero, P. Lio, and Y. Bengio, “Graph attention networks,” *arXiv preprint arXiv:1710.10903*, 2017.
- [3] K. Xu, W. Hu, J. Leskovec, and S. Jegelka, “How powerful are graph neural networks?” *arXiv preprint arXiv:1810.00826*, 2018.
- [4] X. Wang, X. He, M. Wang, F. Feng, and T.-S. Chua, “Neural graph collaborative filtering,” in *Proceedings of the 42nd international ACM SIGIR conference on Research and development in Information Retrieval*, 2019, pp. 165–174.
- [5] W. Hamilton, Z. Ying, and J. Leskovec, “Inductive representation learning on large graphs,” *Advances in neural information processing systems*, vol. 30, 2017.
- [6] S. Wright *et al.*, “The roles of mutation, inbreeding, crossbreeding, and selection in evolution,” 1932.
- [7] C. Darwin, “Origin of the species,” in *British Politics and the environment in the long nineteenth century*. Routledge, 2023, pp. 47–55.
- [8] R. Brady, “Optimization strategies gleaned from biological evolution,” *Nature*, vol. 317, no. 6040, pp. 804–806, 1985.
- [9] A. E. Eiben and C. A. Schippers, “On evolutionary exploration and exploitation,” *Fundamenta Informaticae*, vol. 35, no. 1-4, pp. 35–50, 1998.
- [10] M. Črepinšek, S.-H. Liu, and M. Mernik, “Exploration and exploitation in evolutionary algorithms: A survey,” *ACM computing surveys (CSUR)*, vol. 45, no. 3, pp. 1–33, 2013.
- [11] J. Yu, Y. Zhang, and C. Sun, “Balance of exploration and exploitation: Non-cooperative game-driven evolutionary reinforcement learning,” *Swarm and Evolutionary Computation*, vol. 91, p. 101759, 2024.
- [12] J. H. Holland, “Genetic algorithms,” *Scientific american*, vol. 267, no. 1, pp. 66–73, 1992.
- [13] W. Chao, J. Zhao, L. Jiao, L. Li, F. Liu, and S. Yang, “A match made in consistency heaven: when large language models meet evolutionary algorithms,” *arXiv e-prints*, pp. arXiv–2401, 2024.
- [14] R. Storn and K. Price, “Differential evolution—a simple and efficient heuristic for global optimization over continuous spaces,” *Journal of global optimization*, vol. 11, pp. 341–359, 1997.
- [15] M. Gorges-Schleuter, “Genetic algorithms and population structures,” Ph.D. dissertation, 1991.
- [16] K. R. Opara and J. Arabas, “Differential evolution: A survey of theoretical analyses,” *Swarm and evolutionary computation*, vol. 44, pp. 546–558, 2019.
- [17] V. Ojha, J. Timmis, and G. Nicosia, “Assessing ranking and effectiveness of evolutionary algorithm hyperparameters using global sensitivity analysis methodologies,” *Swarm and Evolutionary Computation*, vol. 74, p. 101130, 2022.

- [18] R. Tanabe and A. Fukunaga, “Reviewing and benchmarking parameter control methods in differential evolution,” *IEEE transactions on cybernetics*, vol. 50, no. 3, pp. 1170–1184, 2019.
- [19] G. Karafotias, M. Hoogendoorn, and Á. E. Eiben, “Parameter control in evolutionary algorithms: Trends and challenges,” *IEEE Transactions on Evolutionary Computation*, vol. 19, no. 2, pp. 167–187, 2014.
- [20] T. Dobzhansky, *Genetics and the Origin of Species*. Columbia university press, 1982, no. 11.
- [21] N. Hansen, S. D. Müller, and P. Koumoutsakos, “Reducing the time complexity of the derandomized evolution strategy with covariance matrix adaptation (cma-es),” *Evolutionary computation*, vol. 11, no. 1, pp. 1–18, 2003.
- [22] X. He, Y. Zhou, Z. Chen, J. Zhang, and W.-N. Chen, “Large-scale evolution strategy based on search direction adaptation,” *IEEE Transactions on Cybernetics*, vol. 51, no. 3, pp. 1651–1665, 2019.
- [23] H. Zhang, J. Sun, K. C. Tan, and Z. Xu, “Learning adaptive differential evolution by natural evolution strategies,” *IEEE Transactions on Emerging Topics in Computational Intelligence*, vol. 7, no. 3, pp. 872–886, 2022.
- [24] X. Cai, L. Gao, and X. Li, “Efficient generalized surrogate-assisted evolutionary algorithm for high-dimensional expensive problems,” *IEEE Transactions on Evolutionary Computation*, vol. 24, no. 2, pp. 365–379, 2019.
- [25] X. Zhou, A. K. Qin, M. Gong, and K. C. Tan, “A survey on evolutionary construction of deep neural networks,” *IEEE Transactions on Evolutionary Computation*, vol. 25, no. 5, pp. 894–912, 2021.
- [26] N. Li, L. Ma, G. Yu, B. Xue, M. Zhang, and Y. Jin, “Survey on evolutionary deep learning: Principles, algorithms, applications, and open issues,” *ACM Computing Surveys*, vol. 56, no. 2, pp. 1–34, 2023.
- [27] M. Pant, H. Zaheer, L. Garcia-Hernandez, A. Abraham *et al.*, “Differential evolution: A review of more than two decades of research,” *Engineering Applications of Artificial Intelligence*, vol. 90, p. 103479, 2020.
- [28] H.-G. Beyer and H.-P. Schwefel, “Evolution strategies—a comprehensive introduction,” *Natural computing*, vol. 1, pp. 3–52, 2002.
- [29] R. Lange, Y. Tian, and Y. Tang, “Large language models as evolution strategies,” in *Proceedings of the Genetic and Evolutionary Computation Conference Companion*, 2024, pp. 579–582.
- [30] H.-G. Beyer and D. V. Arnold, “Theory of evolution strategies—a tutorial,” *Theoretical aspects of evolutionary computing*, pp. 109–133, 2001.
- [31] J. Zhang and A. C. Sanderson, “Jade: adaptive differential evolution with optional external archive,” *IEEE Transactions on evolutionary computation*, vol. 13, no. 5, pp. 945–958, 2009.
- [32] R. Tanabe and A. Fukunaga, “Success-history based parameter adaptation for differential evolution,” in *2013 IEEE congress on evolutionary computation*. IEEE, 2013, pp. 71–78.
- [33] T. Salimans, J. Ho, X. Chen, S. Sidor, and I. Sutskever, “Evolution strategies as a scalable alternative to reinforcement learning,” *arXiv preprint arXiv:1703.03864*, 2017.
- [34] F. Sehnke, C. Osendorfer, T. Rückstieß, A. Graves, J. Peters, and J. Schmidhuber, “Parameter-exploring policy gradients,” *Neural Networks*, vol. 23, no. 4, pp. 551–559, 2010.
- [35] X. He, Z. Zheng, and Y. Zhou, “Mmes: Mixture model-based evolution strategy for large-scale optimization,” *IEEE Transactions on Evolutionary Computation*, vol. 25, no. 2, pp. 320–333, 2020.
- [36] Z. Chen, F. Chen, L. Zhang, T. Ji, K. Fu, L. Zhao, F. Chen, L. Wu, C. Aggarwal, and C.-T. Lu, “Bridging the gap between spatial and spectral domains: A unified framework for graph neural networks,” *ACM Computing Surveys*, vol. 56, no. 5, pp. 1–42, 2023.
- [37] B. Muhammet, R. Guillaume, H. Pierre, G. Benoit, A. Sébastien, and P. Honeine, “When spectral domain meets spatial domain in graph neural networks,” in *Thirty-seventh International Conference on Machine Learning (ICML 2020)-Workshop on Graph Representation Learning and Beyond (GRL+ 2020)*, 2020.
- [38] X. Wang and M. Zhang, “How powerful are spectral graph neural networks,” in *International conference on machine learning*. PMLR, 2022, pp. 23 341–23 362.
- [39] M. Defferrard, X. Bresson, and P. Vandergheynst, “Convolutional neural networks on graphs with fast localized spectral filtering,” *Advances in neural information processing systems*, vol. 29, 2016.

- [40] M. He, Z. Wei, H. Xu *et al.*, “Bernnet: Learning arbitrary graph spectral filters via bernstein approximation,” *Advances in Neural Information Processing Systems*, vol. 34, pp. 14 239–14 251, 2021.
- [41] C. Qian, Y. Yu, K. Tang, Y. Jin, X. Yao, and Z.-H. Zhou, “On the effectiveness of sampling for evolutionary optimization in noisy environments,” *Evolutionary computation*, vol. 26, no. 2, pp. 237–267, 2018.
- [42] C. Qian, Y. Yu, and Z.-H. Zhou, “Analyzing evolutionary optimization in noisy environments,” *Evolutionary computation*, vol. 26, no. 1, pp. 1–41, 2018.
- [43] M. Friedman, “The use of ranks to avoid the assumption of normality implicit in the analysis of variance,” *Journal of the american statistical association*, vol. 32, no. 200, pp. 675–701, 1937.
- [44] J. Kudela, “A critical problem in benchmarking and analysis of evolutionary computation methods,” *Nature Machine Intelligence*, vol. 4, no. 12, pp. 1238–1245, 2022.
- [45] Z. Chen, F. Chen, R. Lai, X. Zhang, and C.-T. Lu, “Rational neural networks for approximating graph convolution operator on jump discontinuities,” in *2018 IEEE International Conference on Data Mining (ICDM)*. IEEE, 2018, pp. 59–68.

# Appendix

For the sake of completeness, we provide additional discussions and module details in the appendices. A summary of the contents is outlined below:

- **Appendix A:** Details of Spectral GNN.
- **Appendix B:** Details of Sampling Function.
- **Appendix C:** Further Experiments.
- **Appendix D:** Invariance Properties of the Adjacency Matrix.
- **Appendix E:** Limitations.

## A Details of Spectral GNN

This section outlines the theoretical foundations and details of spectral GNNs, as illustrated in Figure 1. Spectral GNNs operate in the frequency domain, utilizing the spectral decomposition of the graph Laplacian to formulate convolutional operations. Here, we provide a comprehensive derivation of the spectral formulation.

### A.1 Spectral Convolution and Graph Fourier Transform

Spectral-domain GNNs rely on the graph Fourier transform, which is defined based on the eigen-decomposition of the graph Laplacian. Given a graph  $\mathcal{G} = (\mathbf{V}, \mathbf{E})$  with  $n$  nodes, the symmetric normalized Laplacian is defined as:

$$\mathbf{L} = \mathbf{I} - \mathbf{D}^{-\frac{1}{2}} \mathbf{A} \mathbf{D}^{-\frac{1}{2}} \quad (9)$$

where  $\mathbf{A} \in \mathbb{R}^{n \times n}$  is the adjacency matrix,  $\mathbf{D}$  is the degree matrix, and  $\mathbf{I}$  is the identity matrix. The Laplacian can be decomposed as:

$$\mathbf{L} = \mathbf{U} \mathbf{\Lambda} \mathbf{U}^\top \quad (10)$$

where  $\mathbf{U} \in \mathbb{R}^{n \times n}$  is the matrix of eigenvectors, and  $\mathbf{\Lambda} = \text{diag}(\lambda_1, \lambda_2, \dots, \lambda_n)$  contains the eigenvalues, representing the frequencies of the graph.

The graph Fourier transform of a node feature matrix  $\mathbf{X} \in \mathbb{R}^{n \times f}$  is given by:

$$\hat{\mathbf{X}} = \mathbf{U}^\top \mathbf{X} \quad (11)$$

and the inverse transform is:

$$\mathbf{X} = \mathbf{U} \hat{\mathbf{X}} \quad (12)$$

Spectral convolution is defined as an element-wise product in the frequency domain. For a filter function  $g(\Lambda)$  and node features  $\mathbf{X}$ , the convolution operation is:

$$\mathbf{H} = \mathbf{U}[g(\mathbf{\Lambda}) \odot (\mathbf{U}^\top \mathbf{X})] = \mathbf{U}g(\mathbf{\Lambda})\mathbf{U}^\top \mathbf{X} \quad (13)$$

where  $\odot$  denotes element-wise multiplication, and  $\mathbf{H} \in \mathbb{R}^{n \times f}$  is the filtered node embedding. In our evolutionary algorithm,  $g(\Lambda)$  is designed to emphasize low-frequency components, which capture global correlations among solutions, improving the exploration of the search space.

### A.2 Linear Spectral Filtering

The simplest spectral GNNs use a linear filter function:

$$g(\mathbf{\Lambda}) = \alpha \mathbf{\Lambda} + \beta \quad (14)$$

where  $\alpha$  and  $\beta$  are learnable parameters. The filtered embedding is:

$$\mathbf{H} = \mathbf{U}(\alpha \mathbf{\Lambda} + \beta \mathbf{I})\mathbf{U}^\top \mathbf{X} = (\alpha \mathbf{L} + \beta \mathbf{I})\mathbf{X} \quad (15)$$

This formulation corresponds to a low-pass filter when  $\alpha < 0$ , amplifying low-frequency signals that represent smooth variations across the graph. In our context, such filters help stabilize the evolutionary algorithm by prioritizing global patterns in the solution graph, reducing premature convergence to local optima.

For instance, a simplified form akin to the Graph Convolutional Network (GCN) [1] is given by:

$$g(\Lambda) = 1 - \Lambda \quad (16)$$

yielding:

$$\mathbf{H} = (\mathbf{I} - \mathbf{L})\mathbf{X} = \mathbf{D}^{-\frac{1}{2}}\mathbf{A}\mathbf{D}^{-\frac{1}{2}}\mathbf{X} \quad (17)$$

This operation aligns with our goal of modeling global dependencies, as it aggregates information from direct neighbors while preserving structural coherence.

### A.3 Polynomial Spectral Filtering

To capture more complex frequency patterns, polynomial filters are employed:

$$g(\Lambda) = \sum_{k=0}^K \theta_k \Lambda^k \quad (18)$$

The filtered embedding becomes:

$$\mathbf{H} = \mathbf{U} \left( \sum_{k=0}^K \theta_k \Lambda^k \right) \mathbf{U}^\top \mathbf{X} = \sum_{k=0}^K \theta_k \mathbf{L}^k \mathbf{X} \quad (19)$$

This approach, inspired by Chebyshev-based methods [39], avoids explicit eigendecomposition by expressing the filter as a polynomial of the Laplacian. In our evolutionary algorithm, polynomial filters enable the modeling of higher-order correlations, allowing the algorithm to explore distant relationships in the solution space. For example, a second-order filter ( $K = 2$ ) can be written as:

$$\mathbf{H} = (\theta_0 \mathbf{I} + \theta_1 \mathbf{L} + \theta_2 \mathbf{L}^2) \mathbf{X} \quad (20)$$

where  $\theta_0, \theta_1, \theta_2$  are tuned to balance local and global information.

### A.4 Rational Spectral Filtering

For scenarios requiring precise modeling of abrupt changes in the graph signal (e.g., discontinuities in the fitness landscape), rational filters are used:

$$g(\Lambda) = \frac{\sum_{m=0}^M a_m \Lambda^m}{\sum_{n=0}^N b_n \Lambda^n} \quad (21)$$

The filtered embedding is:

$$\mathbf{H} = \mathbf{U} \left( \frac{P(\Lambda)}{Q(\Lambda)} \right) \mathbf{U}^\top \mathbf{X} = P(\mathbf{L})[Q(\mathbf{L})]^{-1} \mathbf{X} \quad (22)$$

where  $P(\mathbf{L}) = \sum_{m=0}^M a_m \mathbf{L}^m$  and  $Q(\mathbf{L}) = \sum_{n=0}^N b_n \mathbf{L}^n$ . Rational filters, as explored in [45], are computationally intensive but excel at capturing sharp transitions. In our framework, they are applied to detect critical regions in the solution graph, enhancing the evolutionary algorithm's ability to navigate complex fitness landscapes.

Unlike general GNN applications, our spectral GNN framework is tailored to evolutionary algorithms. The spectral filters are optimized to prioritize global correlations, which are critical for guiding the population toward diverse and high-quality solutions. By leveraging low-pass filters (linear or polynomial), we ensure robustness against noise in the fitness evaluations, while rational filters enable precise modeling of complex solution interactions. These adaptations distinguish our approach from prior spectral GNN formulations [36].

## B Details of Sampling Function

This section introduces how  $\psi(\cdot)$  and  $\phi(\cdot)$  in GNE can be viewed as sampling functions. In spectral domain GNNs,  $\phi$  and  $\varphi$  are functions serving as the encoder and decoder, respectively, encoding and decoding the original feature matrix  $\mathbf{X}$ . Consider a simple case where  $\psi(\cdot)$  maps the feature matrix  $\mathbf{X}$  to  $\psi(\mathbf{X})$ , and its parameters are updated by minimizing the loss function  $L$ . The parameter update process in optimization algorithms for the  $k$ -th epoch can be expressed as:

$$\theta_{k+1} = \theta_k - \eta \nabla_{\theta} L(\theta_k), \quad (23)$$

where  $\eta$  is the learning rate, and  $\nabla_{\theta} L(\theta_k)$  is the gradient of the loss function with respect to the parameters  $\theta$ . This update rule represents a standard gradient descent step where the parameters are adjusted in the direction of the negative gradient of the loss function.

### B.1 Feature Update via Backpropagation

As the parameters  $\theta$  are updated, the feature matrix  $\mathbf{X}$  also updates in the feature space. This update process follows the chain rule of backpropagation and can be expressed in terms of  $\theta$  as follows:

$$\mathbf{X}_{k+1} = \mathbf{X}_k - \eta \nabla_{\theta} L(\theta_k) \cdot \nabla_{\theta} \psi, \quad (24)$$

where  $\nabla_{\theta} \psi$  is the gradient of the mapping function  $\psi(\cdot)$  with respect to the parameters  $\theta$ , and  $\nabla_{\theta} L(\theta_k)$  is the gradient of the loss function with respect to the parameters  $\theta$ . The matrix  $\mathbf{X}_k$  represents the feature matrix at  $k$ -th epoch, and this equation represents an update rule for the features in the same way that the parameters are updated. The gradient of the mapping function,  $\nabla_{\theta} \psi$ , influences the change in the feature matrix based on the changes in the model parameters.

### B.2 Assumption of Noisy Gradients

Since gradient estimates are typically noisy, such as in the case of Stochastic Gradient Descent (SGD), these noises are often assumed to follow specific distributions, such as Gaussian or heavy-tailed distributions. Taking the Gaussian distribution as an example, we assume that the noise follows a Gaussian distribution. This implies that both the gradients  $\nabla_{\theta} L(\theta_k)$  and  $\nabla_{\theta} \psi(\mathbf{X}_k)$  are subject to noise modeled as Gaussian distributions with their respective means and covariances. In other words, each gradient is a random variable with a normal distribution, which can be expressed as:

$$\nabla_{\theta} L(\theta_k) \sim \mathcal{N}(\mu_1, \Sigma_1) \quad \text{and} \quad \nabla_{\theta} \psi(\mathbf{X}_k) \sim \mathcal{N}(\mu_2, \Sigma_2), \quad (25)$$

where  $\mu_1$  and  $\mu_2$  are the means, and  $\Sigma_1$  and  $\Sigma_2$  are the covariance matrices of the gradients of the loss function and the mapping function, respectively. The gradient noise model assumes that the gradients are drawn from a normal distribution. The correlation between the gradients of  $L(\theta_t)$  and  $\psi(\mathbf{X}_k)$  is captured by  $\Sigma_{12}$ , which represents the cross-covariance matrix between the two gradients. Thus, we have the following joint distribution for the gradients:

$$\begin{bmatrix} \nabla_{\theta} L(\theta_k) \\ \nabla_{\theta} \psi(\mathbf{X}_k) \end{bmatrix} \sim \mathcal{N} \left( \begin{bmatrix} \mu_1 \\ \mu_2 \end{bmatrix}, \begin{bmatrix} \Sigma_1 & \Sigma_{12} \\ \Sigma_{12}^{\top} & \Sigma_2 \end{bmatrix} \right) \quad (26)$$

### B.3 Gaussian Sampling Process for Feature Update

We now express the feature update rule as a Gaussian sampling process. Given that the gradients are noisy, the update of the feature matrix  $\mathbf{X}_{k+1}$  can be viewed as a random variable that follows a Gaussian distribution, where the mean and covariance of the distribution are derived from the gradients' means and covariances, as well as the matrix  $\mathbf{X}_k$  before the update. Specifically, the expectation of  $\mathbf{X}_{k+1}$  is given by:

$$\mathbb{E}[\mathbf{X}_{k+1}] = \mathbf{X}_k - \eta \mu_1 \cdot \mu_2 \quad (27)$$

The covariance of  $\mathbf{X}_{k+1}$  is determined by the gradients' covariance matrices. Since both gradients contribute to the uncertainty in the update, we can calculate the covariance of  $\mathbf{X}_{k+1}$  as follows:

$$\text{Cov}(\mathbf{X}_{k+1}) = \eta^2 (\Sigma_1 \cdot \mu_2^{\top} + \mu_1 \cdot \Sigma_2 + \Sigma_{12}) \quad (28)$$

Thus, the feature update follows a Gaussian distribution with the following parameters:

$$\mathbf{X}_{k+1} \sim \mathcal{N} \left( \mathbf{X}_k - \eta \mu_1 \cdot \mu_2, \eta^2 (\Sigma_1 \cdot \mu_2^{\top} + \mu_1 \cdot \Sigma_2 + \Sigma_{12}) \right) \quad (29)$$

where  $\mu_1$  and  $\mu_2$  are the expectations of the gradients,  $\Sigma_1$  and  $\Sigma_2$  are the covariance matrices of the gradients, and  $\Sigma_{12}$  represents the cross-covariance between the gradients.

Table 4: Polynomial Bases and Their Expressions

Polynomial Base	Expression	Trend description
<b>Chebyshev</b>	$P_0(x) = 1, P_1(x) = x, P_2(x) = 2x^2 - 1, P_3(x) = 4x^3 - 3x, g(x) = c_0P_0 + c_1P_1 + c_2P_2 + c_3P_3$	Decreases then increases
<b>Bessel</b>	$P_0(x) = 1, P_1(x) = 1 + x, P_2(x) = 1 + 3x + x^2, P_3(x) = 1 + 6x + 6x^2 + x^3, g(x) = c_0P_0 + c_1P_1 + c_2P_2 + c_3P_3$	Monotonically increasing
<b>Bernstein</b>	$P_0(x) = (1 - x)^3, P_1(x) = 3x(1 - x)^2, P_2(x) = 3x^2(1 - x), P_3(x) = x^3, g(x) = c_0P_0 + c_1P_1 + c_2P_2 + c_3P_3$	Decreases then increases
<b>Fibonacci</b>	$P_0(x) = 1, P_1(x) = x, P_2(x) = x^2 + 2x, P_3(x) = x^3 + 3x^2 + x, g(x) = c_0P_0 + c_1P_1 + c_2P_2 + c_3P_3$	Monotonically increasing
<b>Fourier</b>	$g(x) = \frac{a_0}{2} + \sum_{k=1}^3 (a_k \cos(2\pi kx) + b_k \sin(2\pi kx))$	Fluctuates
<b>Gegenbauer</b>	$P_0(x) = 1, P_1(x) = 2\alpha x, P_2(x) = \alpha(2\alpha + 1)x^2 - \alpha, P_3(x) = (2\alpha + 3)(\alpha + 1)x^3 - 3(\alpha + 1)x, g(x) = c_0P_0 + c_1P_1 + c_2P_2 + c_3P_3$	Decreases then increases
<b>Hermite</b>	$P_0(x) = 1, P_1(x) = 2x, P_2(x) = 4x^2 - 2, P_3(x) = 8x^3 - 12x, g(x) = c_0P_0 + c_1P_1 + c_2P_2 + c_3P_3$	Decreases then increases
<b>Jacobi</b>	$P_0(x) = 1, P_1(x) = 0.5(2(\alpha + 1) + (\alpha + \beta + 2)x), P_2(x) = 0.5(\alpha + 1)(\alpha + 2)x^2 + (\alpha + 1)(1 + \beta)x + \dots, g(x) = c_0P_0 + c_1P_1 + c_2P_2 + c_3P_3$	Monotonically increasing
<b>Laguerre</b>	$P_0(x) = 1, P_1(x) = 1 - x, P_2(x) = 0.5(x^2 - 4x + 2), P_3(x) = \frac{x^3 - 9x^2 + 18x - 6}{6}, g(x) = c_0P_0 + c_1P_1 + c_2P_2 + c_3P_3$	Increases then decreases
<b>Legendre</b>	$P_0(x) = 1, P_1(x) = x, P_2(x) = \frac{1}{2}(3x^2 - 1), P_3(x) = \frac{1}{2}(5x^3 - 3x), g(x) = c_0P_0 + c_1P_1 + c_2P_2 + c_3P_3$	Decreases then increases
<b>Lucas</b>	$P_0(x) = 2, P_1(x) = x, P_2(x) = x^2 - 2, P_3(x) = x^3 - 3x, g(x) = c_0P_0 + c_1P_1 + c_2P_2 + c_3P_3$	Decreases then increases
<b>Monomial</b>	$P_0(x) = 1, P_1(x) = x, P_2(x) = x^2, P_3(x) = x^3, g(x) = c_0P_0 + c_1P_1 + c_2P_2 + c_3P_3$	Monotonically increasing

## C Further Experiments

### C.1 Benchmark Functions Used for Optimization Algorithm Evaluation

Table 3: Benchmark Functions Used for Optimization Algorithm Evaluation

Function Name	Expression	Bounds	Dim	Characteristics
Sphere	$f(x) = \sum_{i=1}^n x_i^2$	[-100,100]	30	Smooth, symmetric, and convex; commonly used to test convergence speed toward the origin.
Schwefel	$f(x) = \sum_{i=1}^n  x_i  + \prod_{i=1}^n  x_i $	[-10,10]	30	Discontinuous and complex; tests handling of absolute value and multiplicative interactions.
Schwefel 2.22	$f(x) = \sum_{i=1}^n \left( \sum_{j=1}^i x_j \right)^2$	[-100,100]	30	Similar to Schwefel; evaluates performance on cumulative nonlinear interactions.
Schwefel 2.26	$f(x) = \max_i  x_i $	[-100,100]	30	Tests robustness by focusing on the maximum absolute variable.
Rosenbrock	$f(x) = \sum_{i=1}^{n-1} [100(x_{i+1} - x_i^2)^2 + (x_i - 1)^2]$	[-30,30]	30	"Banana function"; Narrow curved valley; tests local search accuracy and convergence precision.
Quartic	$f(x) = \sum_{i=1}^n ix_i^4 + \text{rand}$	[-1.28,1.28]	30	Unimodal with noise; tests robustness under uncertain environments.
Rastrigin	$f(x) = \sum_{i=1}^n [x_i^2 - 10 \cos(2\pi x_i) + 10]$	[-5.12, 5.12]	30	Multimodal with many local optima; requires balanced exploration and exploitation.
Ackley	$f(x) = -20 \exp \left( -0.2 \sqrt{\frac{1}{n} \sum_{i=1}^n x_i^2} \right) - \exp \left( \frac{1}{n} \sum_{i=1}^n \cos(2\pi x_i) \right) + 20 + \epsilon$	[-32,32]	30	Highly multimodal; flat outer region with sharp minima, tests convergence ability.
Levy	$f(x) = \sum_{i=1}^n \frac{x_i^2}{4000} - \prod_{i=1}^n \cos \left( \frac{x_i}{\sqrt{i}} \right) + 1$	[-600,600]	30	Complex and multimodal; evaluates ability to escape deceptive minima.

Table 3 presents nine standard benchmark functions that are widely used. The single-modal and multi-modal test functions are covered, which can effectively test the performance of the algorithm. In addition, we also add noise and offset to it to test the robustness of the algorithm.

### C.2 Performance of GNE with Different Polynomial Bases

The descriptions of the polynomial bases used in GNE, including their expressions and frequency-weight trends, are provided in Table 4. The performance of GNE across these different polynomial bases, summarized in Table 5, reveals significant variations across benchmark functions. Lower mean

Table 5: GNE Performance Comparison Based on Different Polynomial Bases

GNE+	Sphere	Schwefel	Schwefel 2.22	Schwefel 2.26	Rosenbrock	Quartic	Rastrigin	Ackley	Levy
<b>Chebyshev</b>	<b>3.08E-20</b>	<b>7.46E-10</b>	<b>6.35E-20</b>	<b>6.76E-11</b>	2.85E+01	5.57E-05	<b>0.00E+00</b>	<b>1.29E-10</b>	7.15E-03
<b>Bessel</b>	8.94E-20	1.31E-09	1.98E-19	1.18E-10	2.85E+01	6.94E-05	0.00E+00	2.17E-10	1.56E-02
<b>Fibonacci</b>	8.40E-20	1.25E-09	1.80E-19	1.11E-10	<b>2.85E+01</b>	6.25E-05	0.00E+00	2.05E-10	1.74E-02
<b>Fourier</b>	3.76E-19	8.90E+01	9.24E+03	2.99E+01	5.25E+03	2.45E-01	1.74E+02	1.99E+01	8.33E+00
<b>Gegenbauer</b>	3.39E-20	8.01E-10	7.70E-20	6.98E-11	2.85E+01	6.05E-05	0.00E+00	1.32E-10	1.78E-02
<b>Hermite</b>	4.18E-19	7.53E+01	6.74E+03	2.24E+01	3.40E+03	2.15E-01	1.38E+02	6.57E+00	8.27E+00
<b>Jacobi</b>	7.90E-20	1.23E-09	1.71E-19	1.09E-10	2.85E+01	7.15E-05	0.00E+00	1.94E-10	3.08E-02
<b>Laguerre</b>	1.77E-19	1.88E-09	3.37E-19	1.66E-10	2.85E+01	5.68E-05	0.00E+00	3.17E-10	2.67E-02
<b>Legendre</b>	3.95E-20	8.82E-10	8.66E-20	7.64E-11	2.85E+01	5.26E-05	0.00E+00	1.42E-10	1.61E-02
<b>Lucas</b>	3.82E-19	4.69E+00	3.56E+03	1.42E+01	2.57E+03	2.21E-01	6.95E+01	2.63E+00	6.64E+00
<b>Monomial</b>	7.05E-20	1.14E-09	1.43E-19	1.00E-10	2.85E+01	<b>4.53E-05</b>	0.00E+00	1.89E-10	1.58E-02
<b>Bernstein</b>	3.71E-20	8.30E-10	8.70E-20	7.46E-11	2.85E+01	6.51E-05	0.00E+00	1.42E-10	<b>6.04E-03</b>

values indicate superior optimization efficiency. Among the polynomial bases tested, Chebyshev, Bernstein, and Legendre consistently outperform others, with Chebyshev emerging as the top performer. These three bases share a U-shaped frequency-weight distribution, in which the weights initially decrease and then increase from low to high frequencies. This distribution allows for an effective balance between low-frequency stability and high-frequency diversity, enabling precise and robust optimization. For instance, in functions such as Sphere, Schwefel, and Quartic, these bases yield the smallest mean values, demonstrating their ability to adapt to diverse optimization landscapes. In contrast, polynomial bases such as Bessel, Fibonacci, Jacobi, and Monomial, which emphasize high-frequency components through a monotonic increase in weights, show moderate performance. These bases are well-suited for functions requiring extensive exploration, such as Schwefel and Ackley, where their focus on high-frequency information aids in avoiding local optima. However, their performance on stability-dependent functions like Rosenbrock and Quartic is less consistent, often yielding higher mean values compared to U-shaped bases like Chebyshev and Legendre. Low-frequency dominant bases like Laguerre and Lucas, which feature weights that decrease monotonically from low to high frequencies, offer strong stability but limited exploration capabilities. While they excel in functions such as Sphere and Rosenbrock, where stability is paramount, they struggle in multi-modal or high-complexity functions like Rastrigin and Ackley, where exploration is more critical. This trade-off is evident in their higher mean values in these scenarios. Bases such as Fourier, Gegenbauer, and Hermite, characterized by oscillatory weight distributions, generally perform poorly. Their fluctuating emphasis across frequencies leads to inconsistent results, especially in challenging functions like Schwefel 2.22 and Rastrigin, where balanced filtering is essential. For instance, Fourier demonstrates instability and slow convergence in functions like Schwefel and Ackley, reflecting its inability to balance exploration and exploitation effectively. Overall, the U-shaped frequency-weight distribution of Chebyshev, Bernstein, and Legendre allows them to achieve a superior balance between low-frequency stability and high-frequency diversity, making them the most effective polynomial bases for GNE. Among these, Chebyshev consistently emerges as the best performer, delivering the most stable and accurate results across all benchmark functions. These findings emphasize the importance of selecting a polynomial base with balanced frequency-weight characteristics.

### C.3 The convergence behavior of the population on several representative functions

Figure 5 illustrates the convergence behavior of the population on several representative functions. The first row of the figure presents the 3D visualization form of each function, showing the ups and downs and change trend of the function, and can intuitively see the complexity of different functions and terrain characteristics. The second and third rows are the corresponding contour plots, where the points are biased towards blue for better population fitness and towards red for worse population fitness. By comparison, it can be found that the second row represents the early stage of iteration, and the population is scattered in space, which represents the exploration of the population in the search space. The third row represents that at the later stage of iteration, the population individuals converge relatively centrally to the center, indicating that the algorithm converges well on the function. Overall, the visualization results provide an intuitive basis for evaluating the convergence properties of different algorithms on various functions, and the results show that GNE has an excellent ability to balance exploration and exploitation.

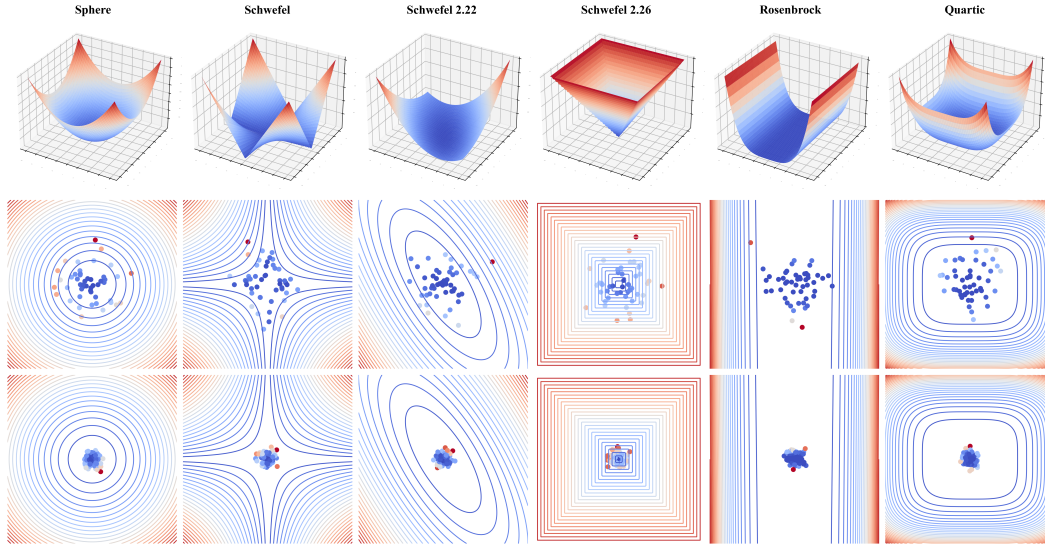


Figure 5: The convergence behavior of the population on several representative functions.

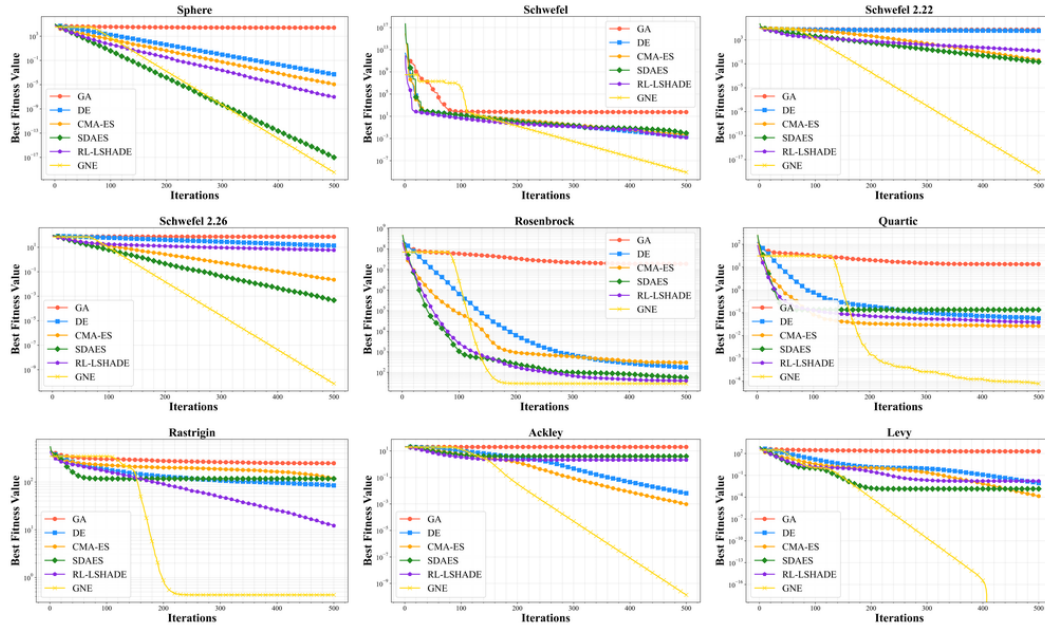


Figure 6: Iterative Convergence Curves of Different Algorithms on Benchmark Functions

#### C.4 Figures Related to Benchmark Algorithm Evaluation (Without Noise)

Figure 6 illustrates the change in the optimal fitness value as the number of iterations increases for six algorithms: GNE, GA, DE, CMA-ES, SDAES, and RL-LSHADE, evaluated on nine noise-free benchmark functions. The results indicate that the GNE algorithm converges rapidly and achieves superior solutions on most functions. In contrast, GA, DE, and other algorithms converge more slowly and exhibit a considerable gap from the optimal value. On the multi-modal Rastrigin function, GNE effectively balances exploration and exploitation, gradually identifying better solutions, whereas other algorithms are prone to falling into local optima. This demonstrates that GNE can explore the solution space more efficiently and locate the global optimum more quickly through its spectrogram decomposition and filtering mechanism.

Figure 7 shows the distribution of the optimal fitness values obtained by the six algorithms on the noiseless benchmark functions. Among these functions, the GNE algorithm exhibits outstanding

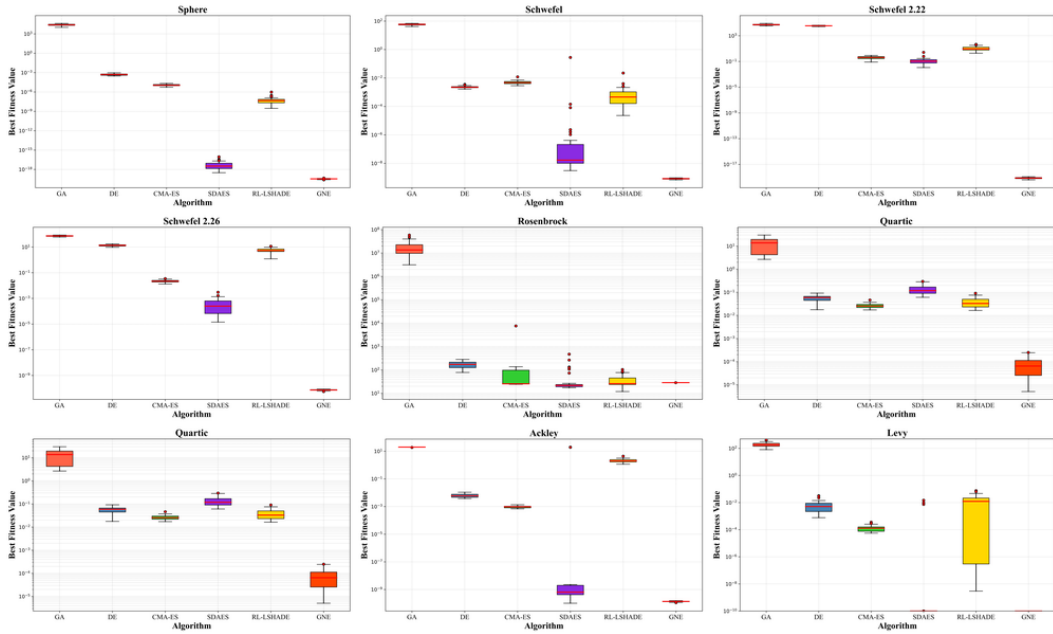


Figure 7: Boxplots of Different Algorithms on Benchmark Functions

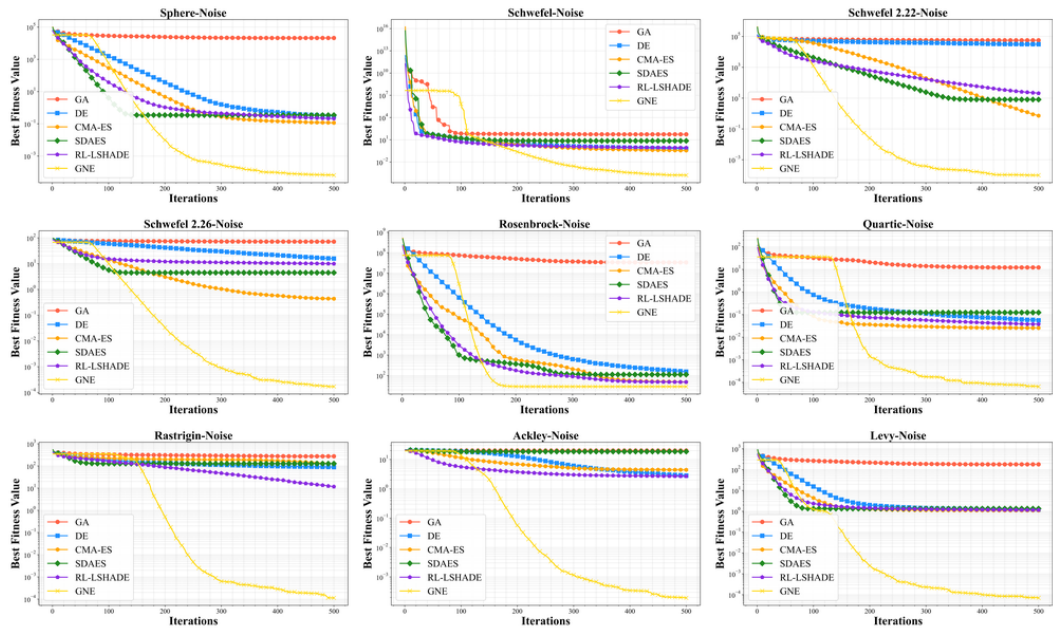


Figure 8: Iterative Convergence Curves of Different Algorithms on Noisy Benchmark Functions

performance. For example, in the Sphere function, GNE yields a narrow box range and a low median, indicating that its optimal fitness values across multiple runs are concentrated and demonstrate high stability. In contrast, GA produces a wider box range, more significant fluctuations, and poor stability. On the Rosenbrock function, GNE also demonstrates strong stability. Although SDAES and some other algorithms may obtain better solutions in certain runs, their overall data distribution is more dispersed and less stable than that of GNE. These results clearly show that GNE maintains consistent performance and effectively reduces the influence of stochastic factors when addressing various types of optimization problems.

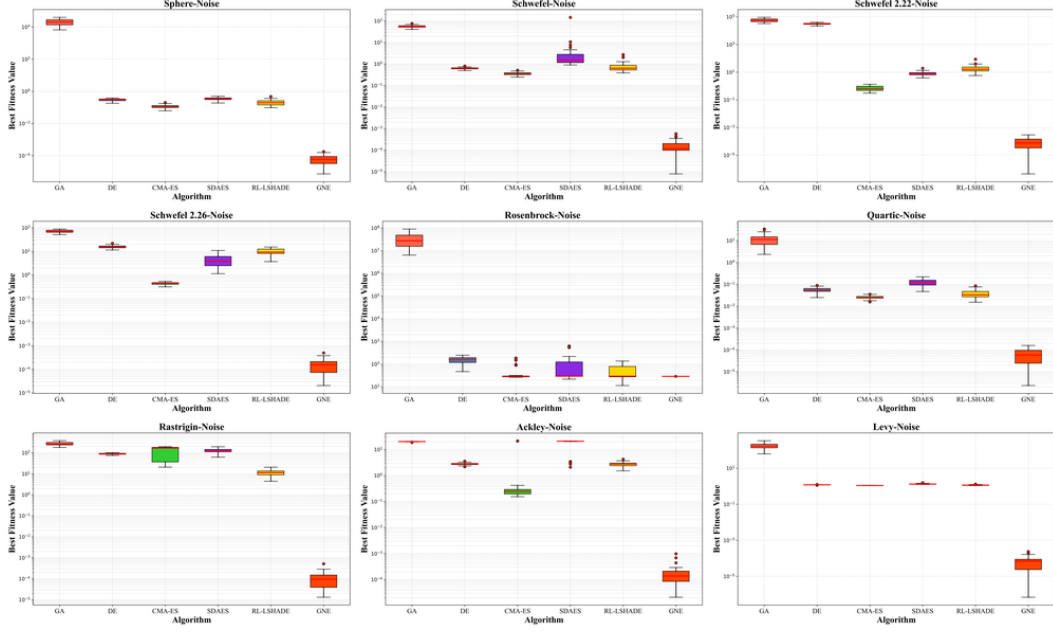


Figure 9: Boxplots of Different Algorithms on Noisy Benchmark Functions

### C.5 Figures Related to Benchmark Algorithm Evaluation (With Noise)

Figure 8 and Figure 9 present the iterative convergence curves and the boxplot results in a noisy environment. The GNE algorithm demonstrates strong noise resistance and robust performance. Compared with other algorithms, it exhibits clear advantages in both convergence speed and solution stability. This performance can be attributed to the design in which the population is modeled as a graph structure and optimized through spectral analysis. This approach enables the algorithm to effectively extract valuable genetic information while filtering out noise interference in complex noisy optimization scenarios. As a result, the GNE algorithm achieves accurate and stable optimization, providing a reliable solution for addressing optimization problems affected by noise in practical applications.

## D Invariance Properties of the Adjacency Matrix

In this section, we demonstrate the invariance properties of the adjacency matrix  $\mathbf{A}$ , which is computed using the cosine similarity between individuals  $i$  and  $j$ , based on their difference vectors  $\mathbf{z}_i = \mathbf{x}_i - \mathbf{x}_0$ . We prove that this adjacency matrix remains invariant under translation, rotation, and scaling transformations applied to the population  $\mathbf{X}$ . These invariance properties ensure that the adjacency matrix  $\mathbf{A}$  robustly captures the relationships between individuals in the population, regardless of the transformation applied to the entire population.

The adjacency matrix is given by:

$$\mathbf{A}_{ij} = \frac{\mathbf{z}_i \cdot \mathbf{z}_j^\top}{\|\mathbf{z}_i\| \|\mathbf{z}_j\|}. \quad (30)$$

where  $\mathbf{z}_i = \mathbf{x}_i - \mathbf{x}_0$  is the difference vector for individual  $i$ , and  $\|\mathbf{z}_i\|$  denotes the Euclidean norm of the difference vector.

We will now demonstrate that this matrix remains invariant under translation, rotation, and scaling transformations.

### D.1 Translation Invariance

Consider a translation transformation where every individual in the population is shifted by a constant vector  $\mathbf{\Delta}$ , such that the new population is:

$$\tilde{\mathbf{x}}_i = \mathbf{x}_i + \mathbf{\Delta} \quad \forall i. \quad (31)$$

Under this transformation, the difference vectors become:

$$\tilde{\mathbf{z}}_i = \tilde{\mathbf{x}}_i - \mathbf{x}_0 + \mathbf{\Delta} = \mathbf{x}_i - \mathbf{x}_0 = \mathbf{z}_i, \quad (32)$$

which means the difference vectors remain the same after translation. Since the cosine similarity only depends on the difference vectors, the similarity matrix  $\mathbf{a}_{ij}$  does not change under translation:

$$\tilde{\mathbf{A}}_{ij} = \frac{\tilde{\mathbf{Z}}_i \cdot \tilde{\mathbf{Z}}_j}{\|\tilde{\mathbf{Z}}_i\| \|\tilde{\mathbf{Z}}_j\|} = \frac{\mathbf{Z}_i \cdot \mathbf{Z}_j}{\|\mathbf{Z}_i\| \|\mathbf{Z}_j\|} = \mathbf{A}_{ij}. \quad (33)$$

Therefore, the adjacency matrix is invariant under translation.

## D.2 Rotation Invariance

Next, consider a rotation transformation that applies a rotation matrix  $\mathbf{R}$  to the entire population. The new coordinates of the individuals are:

$$\tilde{\mathbf{x}}_i = \mathbf{R}\mathbf{x}_i \quad \forall i. \quad (34)$$

The difference vectors after rotation become:

$$\tilde{\mathbf{z}}_i = \tilde{\mathbf{x}}_i - \mathbf{x}_0 = \mathbf{R}\mathbf{x}_i - \mathbf{R}\mathbf{x}_0 = \mathbf{R}(\mathbf{x}_i - \mathbf{x}_0) = \mathbf{R}\mathbf{z}_i. \quad (35)$$

Now, we need to check if the cosine similarity remains the same after rotation. The cosine similarity between two difference vectors  $\mathbf{Z}_i$  and  $\mathbf{Z}_j$  after rotation is:

$$\tilde{\mathbf{A}}_{ij} = \frac{\tilde{\mathbf{Z}}_i \cdot \tilde{\mathbf{Z}}_j}{\|\tilde{\mathbf{Z}}_i\| \|\tilde{\mathbf{Z}}_j\|}. \quad (36)$$

Substituting  $\tilde{\mathbf{Z}}_i = \mathbf{R}\mathbf{Z}_i$  and  $\tilde{\mathbf{Z}}_j = \mathbf{R}\mathbf{Z}_j$ , we have:

$$\tilde{\mathbf{A}}_{ij} = \frac{(\mathbf{R}\mathbf{Z}_i) \cdot (\mathbf{R}\mathbf{Z}_j)}{\|\mathbf{R}\mathbf{Z}_i\| \|\mathbf{R}\mathbf{Z}_j\|}. \quad (37)$$

Since  $\mathbf{R}$  is a rotation matrix, it is orthogonal, meaning that  $\mathbf{R}^\top \mathbf{R} = \mathbf{I}$ , and therefore it preserves the inner product:

$$(\mathbf{R}\mathbf{z}_i) \cdot (\mathbf{R}\mathbf{z}_j) = \mathbf{z}_i \cdot \mathbf{z}_j. \quad (38)$$

Also, since  $\mathbf{R}$  is orthogonal, it preserves the norm:

$$\|\mathbf{R}\mathbf{z}_i\| = \|\mathbf{z}_i\| \quad \text{and} \quad \|\mathbf{R}\mathbf{z}_j\| = \|\mathbf{z}_j\|. \quad (39)$$

Thus, we can simplify the expression for  $\tilde{\mathbf{a}}_{ij}$  as follows:

$$\tilde{\mathbf{A}}_{ij} = \frac{\mathbf{Z}_i \cdot \mathbf{Z}_j}{\|\mathbf{Z}_i\| \|\mathbf{Z}_j\|} = \mathbf{A}_{ij}. \quad (40)$$

Therefore, the adjacency matrix is invariant under rotation.

## D.3 Scaling Invariance

Finally, consider a scaling transformation where every individual in the population is scaled by a constant factor  $\alpha$ , such that the new population is:

$$\tilde{\mathbf{x}}_i = \alpha \mathbf{x}_i \quad \forall i. \quad (41)$$

The difference vectors after scaling become:

$$\tilde{\mathbf{z}}_i = \tilde{\mathbf{x}}_i - \mathbf{x}_0 = \alpha \mathbf{x}_i - \alpha \mathbf{x}_0 = \alpha(\mathbf{x}_i - \mathbf{x}_0) = \alpha \mathbf{z}_i. \quad (42)$$

The norm of a vector scales by  $\alpha$ , so we have:

$$\|\tilde{\mathbf{z}}_i\| = \|\alpha \mathbf{z}_i\| = \alpha \|\mathbf{z}_i\|. \quad (43)$$

Thus, the cosine similarity between two difference vectors  $\tilde{\mathbf{z}}_i$  and  $\tilde{\mathbf{z}}_j$  after scaling is:

$$\tilde{\mathbf{A}}_{ij} = \frac{\tilde{\mathbf{Z}}_i \cdot \tilde{\mathbf{Z}}_j}{\|\tilde{\mathbf{Z}}_i\| \|\tilde{\mathbf{Z}}_j\|} = \frac{(\alpha \mathbf{Z}_i) \cdot (\alpha \mathbf{Z}_j)}{\alpha \|\mathbf{Z}_i\| \alpha \|\mathbf{Z}_j\|} = \frac{\mathbf{Z}_i \cdot \mathbf{Z}_j}{\|\mathbf{Z}_i\| \|\mathbf{Z}_j\|} = \mathbf{A}_{ij}. \quad (44)$$

Therefore, the adjacency matrix is invariant under scaling.

## **E Limitations**

Despite the effectiveness of GNE, there are several limitations in this study. First, GNE models the adjacency matrix based on individual similarities and obtains frequency components through the diagonalization of the Laplacian matrix. Although GNE outperforms other algorithms on benchmark functions, its runtime is moderate and can be improved. As the problem dimensionality and population size increase, the computational cost of the adjacency matrix and spectral decomposition grows, which has not been addressed in this study. To address this, future work will explore adaptive population reduction strategies to optimize runtime during GNE iterations. Additionally, the filter function used in this study is relatively simple, and we have not systematically examined the impact of different polynomial bases or filter forms, such as linear filters, rational filters, and other nonlinear filters. Furthermore, while EAs should enhance exploration in the early stages and exploitation in the later stages of evolution, adaptive filters in GNE that change throughout the iteration process have not been discussed. Future work will focus on exploring a broader range of filter forms and conducting systematic analysis of their impact on GNE performance. Finally, GNE has not yet been evaluated on real-world optimization problems. Future evaluations may consider engineering optimization tasks, as well as neural network parameter and structure optimization, to assess GNE's performance in practical applications.